Vol 18 No 3, March 2009
1674-1056/2009/18(03)/0958-11
Chinese Physics B
© 2009 Chin. Phys. Soc.
and IOP Publishing Ltd

Regular nonlinear response of the driven Duffing oscillator to chaotic time series*

Yuan Ye(袁 野)[a], Li Yue(李 月)[a]†, Danilo P. Mandic[b], and Yang Bao-Jun(杨宝俊)[c]

[a] *School of Communication Engineering, Jilin University, Changchun* 130012, *China*
[b] *Department of Electrical and Electronic Engineering, Imperial College, London SW72BT, UK*
[c] *Department of Geophysics, Jilin University, Changchun* 130026, *China*

(Received 16 July 2008; revised manuscript received 28 August 2008)

Nonlinear response of the driven Duffing oscillator to periodic or quasi-periodic signals has been well studied. In this paper, we investigate the nonlinear response of the driven Duffing oscillator to non-periodic, more specifically, chaotic time series. Through numerical simulations, we find that the driven Duffing oscillator can also show regular nonlinear response to the chaotic time series with different degree of chaos as generated by the same chaotic series generating model, and there exists a relationship between the state of the driven Duffing oscillator and the chaoticity of the input signal of the driven Duffing oscillator. One real-world and two artificial chaotic time series are used to verify the new feature of Duffing oscillator. A potential application of the new feature of Duffing oscillator is also indicated.

Keywords: Duffing oscillator, chaotic time series, phase plane diagram, largest Lyapunov exponent

PACC: 0545

1. Introduction

Since in 1963 Lorenz firstly described chaos[1] and tried to model weather patterns by a system of coupled differential equations known as the Lorenz equations, the research on chaos has drawn increasingly great attention.[2−7] A chaotic system is sensitive to regular signals but immune to noise. When the system is in the critical state, a small perturbation of the system may lead to the change of the state of the system.[8] It is now widely agreed that a dynamic system can be called chaotic only if it exhibits the property of sensitive dependence on initial conditions (SDIC).[9] The property of SDIC of a chaotic system has been applied for the detection of a weak signal. In 1992, Birx and Pipenberg firstly developed a complex-mapping-feed-forward-networks (CMFFNS) in conjunction with Duffing oscillator to detect signals in noise environments.[10] In 1999, Wang *et al* investigated more deeply the method for the detection of weak signals buried in strong noise based on the bifurcation behaviour of the driven Duffing oscillator, the detection limit in signal-to-noise (SNR) ratio reached –68 dB.[11] Then Wang *et al* proposed a method for estimating the amplitude and phase of a weak signal based on the intermittent state transition in Duffing oscillator.[12,13]

The driven Duffing oscillator mentioned above can be described by

$$\ddot{y} + \alpha\dot{y} - y + y^3 = \gamma\cos(\omega t) + x(t), \qquad (1)$$

where α is the damping ratio, $-y + y^3$ is the nonlinear restoring force, $\gamma\cos(\omega t)$ is the build-in signal and $x(t)$ is the detected weak signal. In 2003, Li and Yang developed a modified Duffing oscillator for detecting weak signals buried in strong noise,[14] that is

$$\ddot{y} + \alpha\dot{y} - y^3 + y^5 = \gamma\cos(\omega t) + x(t), \qquad (2)$$

which has a higher order nonlinear restoring force, i.e., $-y^3 + y^5$, compared with the normal Duffing oscillator. The modified Duffing oscillator has an improved property of SDIC, and a lower limiting detection SNR ratio up to –91dB was obtained based on the modified Duffing oscillator.[14] Later Li *et al* also discussed the application of the modified Duffing oscillator in seismic signal processing.[15,16]

The common features of the researches mentioned above are that they all made use of the property of SDIC of the normal or modified driven Duffing oscillator, and the detected signals were all periodic or quasi-periodic. Therefore, it is natural to consider how about the results if the detected signal ($x(t)$ in Eqs.(1)

*Project supported by the National Natural Science Foundation of China (Grant Nos 40574051 and 40774054).
†Corresponding author. E-mail: liyue84@gmail.com

and (2)) is aperiodic, or even in a more complex case, chaotic? In practice, a great many kinds of signals are not regular, for example, the physiological signals such as hand tremor, electrocardiograph (ECG), electroencephalogram (EEG), heart rate variability (HRV), are aperiodic, even chaotic.[17−19]

We found during research that the chaotic time series could make Duffing oscillator generate phase plane diagrams with different degrees of chaos, and there exists a relationship between the degree of chaos of the input signals and the degree of chaos of the phase plane of Duffing oscillator. This potential feature makes it possible to apply Duffing oscillator to deal with non-periodic signals. We will make use of two kinds of artificial and one real-world chaotic time series to verify the new feature of Duffing oscillator. EEG signals, which have been widely proved to be chaotic time series,[20−22] are employed as real-world signals to verify the new feature of Duffing oscillator. Moreover, based on the results of the numerical experiments on normal and epileptic EEG signals, an initial method based on the new feature of Duffing oscillator is proposed to detect epileptic seizure, which indicates the applicability of the new feature of Duffing oscillator.

This paper is organized as follows: Section 2 describes the time series for testing; Section 3 gives the results of numerical experiments of testing the new feature of the driven Duffing oscillator; Section 4 contains discussions; Section 5 introduces a potential application of the new feature of the driven Duffing oscillator; Section 6 gives the conclusion.

2. Testing chaotic time series

2.1. Artificial chaotic time series

In this paper, the new feature of Duffing oscillator is verified by three kinds of chaotic time series, two of which are the time series generated by artificial mathematical models and the remaining one is a real-world chaotic time series. The first kind of chaotic time series is generated by Hénon map, described as

$$\begin{aligned} x_{n+1} &= y_n + 1 - a \cdot x_n^2, \\ y_{n+1} &= b \cdot x_n. \end{aligned} \tag{3}$$

Hénon map is related with the parameters a and b, usually set at $a = 1.4$ and $b = 0.3$.[23] The second artificial chaotic time series is the output of Logistic map, shown by

$$x_{n+1} = kx_n(1 - x_n),\ x \in (0,\ 1),\ k \in [1,\ 4]. \tag{4}$$

Logistic map is only related with the bifurcation parameter k. When $k \in [3.569,\ 4]$, Logistic map is in chaotic state.[24] These two artificial chaotic time series generating models (CTSGMs) are used to generate 120000 sample points with the sampling interval 0.005.

2.2. Real-world chaotic time series

The real-world chaotic time series used for verifying the new feature of the driven Duffing oscillator are the normal and epileptic time series. The raw EEG time series used in this paper were recorded according to the International Standard 10∼20 system. Data were digitized with a 12-bit analogue-to-digital converter at a sampling rate of 200 Hz and stored on a hard disk. We recorded 80-second-long EEG data, thus getting 16 000 sample points for each channel. Four groups of EEG time series were obtained, two of which were recorded from two healthy persons, and the remaining two were recorded from two epileptic patients. Volunteers were relaxed in an awake state with eyes closed. The epileptic EEG signals were recorded for patients during induced epileptic seizure. It has been widely accepted that the largest Lyapunov exponent (LLE) of EEG time series during seizure descends,[21] i.e. normal and epileptic EEG time series have different chaoticity.

3. Numerical experiments

As the modified Duffing oscillator shows improved SDIC, in this paper, all the numerical experiments are done based on the modified Duffing oscillator, and all Duffing oscillator mentioned below refers to the modified Duffing oscillator. Figure 1 shows the block diagram of the driven Duffing oscillator. We use the following steps to verify the new feature of Duffing oscillator: firstly, adjust the amplitude γ of the built-in signal $\gamma\cos(\omega t)$ of Duffing oscillator without input signal $x(t)$ to make Duffing oscillator in critical chaotic state, the value of γ we obtained here is $\gamma = 0.7256$. Then put the testing time series into Duffing oscillator as input signal, and solve the Duffing equation by the fourth-order Runge–Kutta algorithm to get the numerical solutions; finally the states of Duffing oscillator can be shown by the output signals of Duffing

oscillator, the phase plane diagram or Poincaré section diagram.

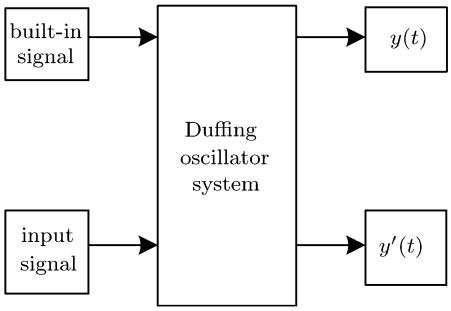


Fig.1. Block diagram of the driven Duffing oscillator.

3.1. Artificial chaotic time series

The testing chaotic time series are put into Duffing oscillator. For Hénon map, two groups of parameters are taken respectively to generate different testing time series, $a = 1.4$, $b = 0.1$ for $H_1(t)$ and $a = 1.4$, $b = 0.3$ for $H_2(t)$. $H_1(t)$ and $H_2(t)$ are put into Duffing oscillator as input signal respectively. Then the corresponding phase plane diagrams of Duffing oscillator can be obtained. As shown in Fig.2, we note that there exists obvious difference between the phase plane diagrams corresponding to $H_1(t)$ and $H_2(t)$. The phase plane diagram corresponding to $H_2(t)$ is more chaotic than that corresponding to $H_1(t)$, in other words, the phase plane diagram corresponding to $H_1(t)$ is closer to periodicity.

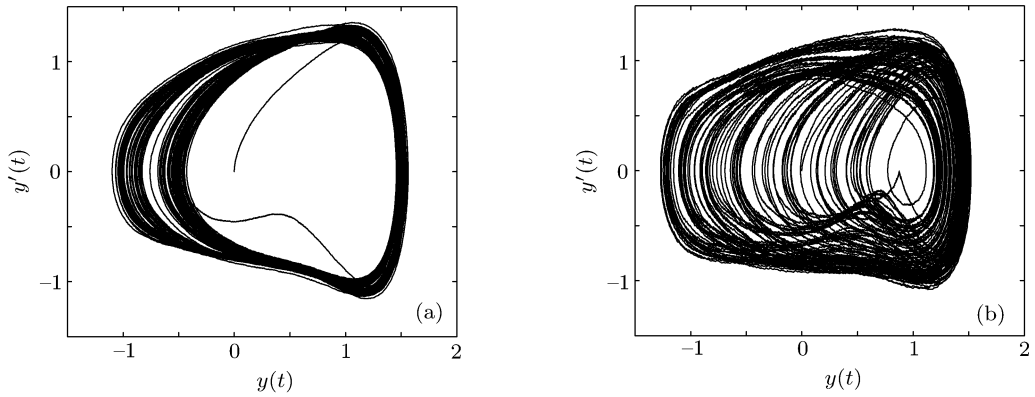


Fig.2. Phase plane diagrams of the driven Duffing oscillator obtained with (a) $H_1(t)$ and (b) $H_2(t)$ as input signal respectively.

Similarly, for Logistic map, different bifurcation parameters $k = 3.7$ and $k = 4$ are taken respectively in order to get two groups of output signals of Logistic map, $L_1(t)$ and $L_2(t)$. The phase plane diagrams corresponding to $L_1(t)$ and $L_2(t)$ are shown in Fig.3, from which it can be seen that the phase plane diagram corresponding to $L_2(t)$ is more chaotic than that corresponding to $L_1(t)$.

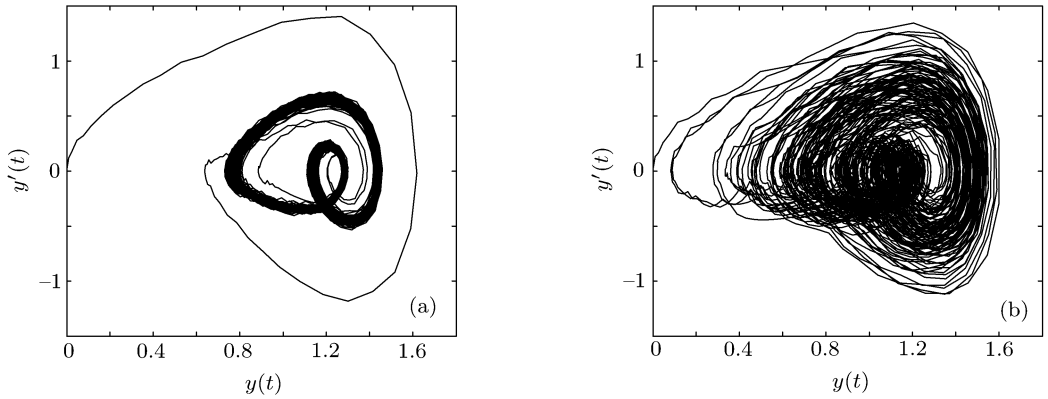


Fig.3. Phase plane diagrams of the driven Duffing oscillator obtained with (a) $L_1(t)$ and (b) $L_2(t)$ as input signal respectively.

Based on Fig.2 and Fig.3, we find that the phase plane results are similar for the two kinds of testing chaotic time series, namely that Duffing oscillator shows phase plane diagrams with different degree of chaos in both cases . When $H_1(t)$ and $L_1(t)$ are as input signals respectively, the Duffing oscillator are in chaotic state, yet the phase plane diagrams are close to periodicity to some extent (shown in Fig.2(a) and Fig.3(a)). When $H_2(t)$ and $L_2(t)$ are as input signals respectively, the orbits of phase planes of Duffing oscillator are more chaotic, in summary, the degree of chaos is higher (shown in Fig.2(b) and Fig.3(b)).

3.2. Real-world time series

In this paper, EEG time series are employed as real-world time series to verify the new feature of Duffing oscillator. It has been widely proved that the LLE value of EEG time series during epileptic seizure is smaller than that of normal EEG time series,[20−22] which means that the degree of chaos of epileptic EEG time series is weaker than that of normal EEG time series.

Normal and epileptic EEG signals are put into Duffing oscillator as input signal respectively. Then the corresponding phase plane diagrams of Duffing oscillator can be obtained. As shown in Fig.4, for both normal and epileptic EEG signals, Duffing oscillator shows chaotic phase plane, but there exists obvious difference between the phase plane diagrams corresponding to normal and epileptic EEG signals. The orbit of the phase plane corresponding to the normal EEG signal covers a small zone, concentrates around a 'core', and is more chaotic, whereas the orbit of the phase plane corresponding to the epileptic EEG signal covers a larger zone, and is smooth and more ordered comparatively. It can be seen that the real-world time series with different degree of chaos also lead the driven Duffing oscillator to different states.

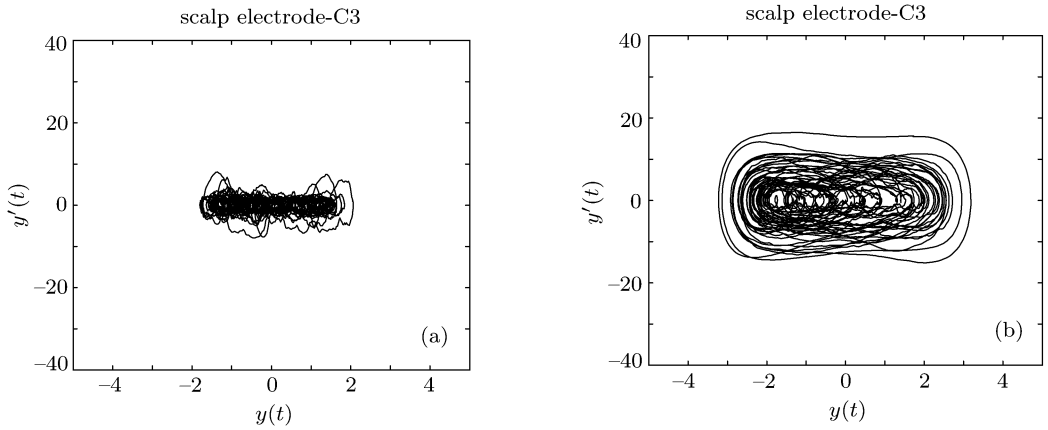


Fig.4. Phase plane diagrams of the driven Duffing with (a) normal EEG time series and (b) epileptic EEG time series as input signal respectively. The normal and epileptic EEG signals were taken from the scalp electrode with the same index, C3.

4. Discussion

4.1. Analysis of the results of numerical experiments by LLE

An important parameter for describing the nonlinear dynamical behaviour of a chaotic oscillator is the largest Lyapunov exponent,[25] which is used in this paper as a quantitative indicator of degree of chaos of a chaotic time series. A positive LLE means that the system exhibits chaotic behaviour and the orbit is unstable, whereas a negative LLE indicates the orbit is attracted to a stable fixed point or stable periodic orbit. Negative Lyapunov exponents are characteristic of dissipative or non-conservative systems. The LLE is employed in this paper to make a quantitative analysis on the chaoticity of a time series.

The LLEs of the input and output signals of the driven Duffing oscillator are computed. The LLEs of the output signals of the driven Duffing oscillator can indicate the state of the driven Duffing oscillator. The LLE results of $H_1(t)$, $H_2(t)$, $L_1(t)$, $L_2(t)$ and the corresponding $y(t)$ are shown in Table 1. It can be seen that all the LLE values are positive, which indicates that all the analysed signals are chaotic time series. The LLE value of $y(t)$ with $H_1(t)$ as input sig-

nal is smaller than that of $y(t)$ with $H_2(t)$ as input signal, which shows that the Duffing oscillator with $H_2(t)$ as input signal is in a more chaotic state than that with $H_1(t)$ as input signal. At the same time, we note that the LLE value of $H_1(t)$ is smaller than that of $H_2(t)$. The phenomena described above still occur when $L_1(t)$ and $L_2(t)$ are used as input signals of Duffing oscillator respectively. Therefore, we can summarize that the output signals with different degree of chaos generated by the same CTSGM can lead to Duffing oscillator in different states, and the higher the degree of chaos of the input signal of Duffing oscillator, the more chaotic the state of the Duffing oscillator.

Table 1. LLEs for $H_1(t)$, $H_2(t)$, $L_1(t)$, $L_2(t)$ and the corresponding output signals of the driven Duffing oscillator.

input signal of Duffing oscillator	LLE	
		$y(t)$
$H_1(t)$	0.3187	0.0132
$H_2(t)$	0.4215	0.0364
$L_1(t)$	0.3459	0.0109
$L_2(t)$	0.6932	0.0372

The LLE values of normal and epileptic EEG signals and the corresponding output signals $y(t)$ of Duffing oscillator are shown in Table 2. It can be seen that all the LLE values are positive, which indicates that they are chaotic time series. The LLE value of $y(t)$ corresponding to the normal EEG signal is larger than that of $y(t)$ corresponding to the epileptic EEG signal, which implies that the Duffing oscillator with normal EEG signal as input signal is in a more chaotic state than the Duffing oscillator with epileptic EEG signal as input signal. Moreover, the LLE value of the normal EEG signal is larger than that of the epileptic EEG signal, which also shows that the input signal of higher degree of chaos induces the corresponding Duffing oscillator to more chaotic state. This is consistent with the results of the verification of the new feature of the driven Duffing oscillator by the artificial time series.

Table 2. LLEs for normal and epileptic EEG signals and the corresponding output signals of the driven Duffing oscillator.

input signal of Duffing oscillator	LLE	
		$y(t)$
normal EEG	0.2355	0.1726
epileptic EEG	0.0833	0.0623

4.2. Influence of the amplitude of input signals on the state of Duffing oscillator

In the experiment, we note that the amplitude of $H_1(t)$ is smaller than that of $H_2(t)$ (shown in Fig.5), therefore, it is needed to consider whether the difference between the phase plane diagrams of Duffing oscillator with $H_1(t)$ and $H_2(t)$ as input signal respectively only resulted from the difference in amplitudes between $H_1(t)$ and $H_2(t)$. The influence of amplitude of the input signal on the phase plane of Duffing oscillator is discussed below.

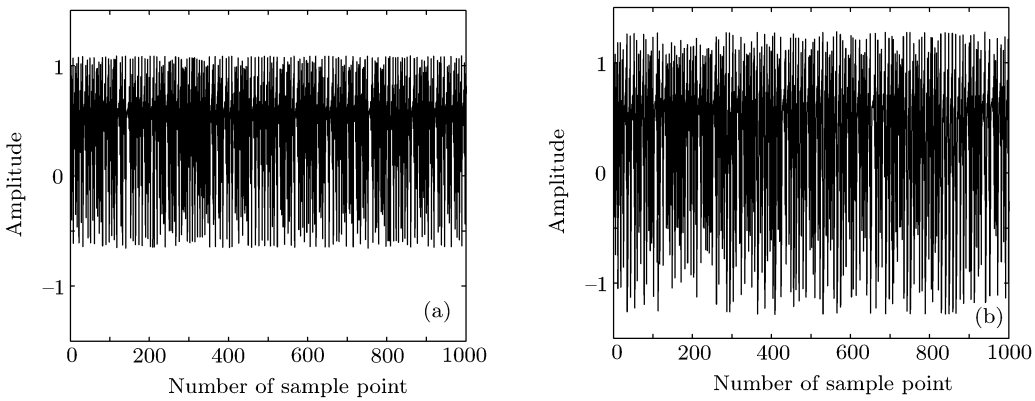


Fig.5. Output time series of Hénon map with different parameters, (a) $H_1(t)$ obtained with $a = 1.4$ and $b = 0.1$, (b) $H_2(t)$ obtained with $a = 1.4$ and $b = 0.3$.

We use the following steps to survey the influence of the amplitude of the input signal on the state of Duffing oscillator. $H_1(t)$, which is of smaller amplitude, is multiplied by the coefficient α to have the same average value of amplitude as $H_2(t)$. Then $\alpha \cdot H_1(t)$ is put into Duffing oscillator as input signal

to get the phase plane diagram, which is to be compared with that of the Duffing oscillator with $H_2(t)$ as input signal. Before the experiment, it is needed to ensure that the coefficient α has no influence on the chaoticity of $H_1(t)$. It is proved below that the LLE value of $H_1(t)$ does not change after being multiplied by the coefficient α.

Based on the steps for calculating LLE,[25] the vector $\boldsymbol{X}_j$ is multiplied by the coefficient α, that is,

$$\begin{aligned}\alpha \cdot \boldsymbol{X}_j =& \alpha \cdot [x_1, x_2, x_3, \ldots, x_{i+m-1}] \\ =& [\alpha x_1, \alpha x_2, \alpha x_3, \ldots, \alpha x_{i+m-1}],\end{aligned}$$

hence the vector distance is $D_= |\alpha \boldsymbol{X}_j - \alpha \boldsymbol{X}_i| = \alpha \cdot |\boldsymbol{X}_j - \boldsymbol{X}_i| = \alpha \cdot d$, then the LLE L_α of $\alpha \cdot H_1(t)$ can be written as:

$$\begin{aligned}L_\alpha =& \frac{1}{n-m} \sum_{i-1}^{n-m} \frac{1}{t} \mathrm{lb}_2 \frac{D_{i+1}}{D_i} \\ =& \frac{1}{n-m} \sum_{i-1}^{n-m} \frac{1}{t} \mathrm{lb}_2 \frac{\alpha \cdot d_{i+1}}{\alpha \cdot d_i} \\ =& \frac{1}{n-m} \sum_{i-1}^{n-m} \frac{1}{t} \mathrm{lb}_2 \frac{d_{i+1}}{d_i},\end{aligned}$$

and the LLE L_1 of $H_1(t)$ is:

$$L_1 = \frac{1}{n-m} \sum_{i-1}^{n-m} \frac{1}{t} \mathrm{lb}_2 \frac{d_{i+1}}{d_i},$$

therefore, $L_\alpha = L_1$. That is, the nonlinear dynamic characteristic of $H_1(t)$ does not change after being multiplied by the coefficient α.

Next, we plot the phase plane diagram of Duffing oscillator with $\alpha \cdot H_1(t)$ as input signal. Firstly, the average value of the amplitude $A_2 = \dfrac{\left| \sum_{t=0}^{T} H_2(t) \right|}{T}$ of $H_2(t)$ is computed and $A_2 = 0.6772$ is obtained. In a similar way, the average value of the amplitude of $H_1(t)$ is obtained as $A_1 = 0.6062$. Then, $H_1(t)$ is multiplied by the amplitude factor $\alpha = \dfrac{A_2}{A_1} = 1.1172$ to make $\alpha \cdot H_1(t)$ have the same average value of amplitude as $H_2(t)$. Finally, $\alpha \cdot H_1(t)$ is put into Duffing oscillator as input signal and the corresponding phase plane diagram is obtained as shown in Fig.6. There exist some slight differences of the orbits between the phase plane diagrams corresponding to $\alpha \cdot H_1(t)$ and $H_1(t)$ (Fig.6 and Fig.2(a)), which we think are reasonable. After all, the amplitudes of $\alpha \cdot H_1(t)$ and $H_1(t)$ are different, and because of the property of SDIC of Duffing oscillator, the change of the amplitude of the driving signal must have an influence on the state of Duffing oscillator. But in general, the phase plane diagram of Duffing oscillator with $\alpha \cdot H_1(t)$ as input signal keeps basically consistent with that of Duffing oscillator with $H_1(t)$ as input signal, and is different from that corresponding to $H_2(t)$. The change of the amplitude of the input signal in a limited range has little influence on the state of Duffing oscillator. Hence, the difference of degree of chaos of phase plane diagram of Duffing oscillator with $H_1(t)$ and $H_2(t)$ as input signal respectively has not resulted from the difference in amplitude between $H_1(t)$ and $H_2(t)$.

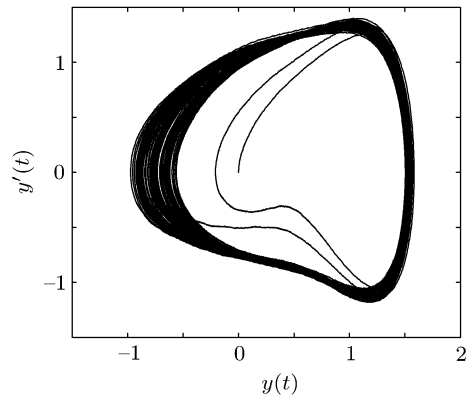


Fig.6. Phase plane diagram of the driven Duffing oscillator with $\alpha \cdot H_1(t)$ as input signal.

4.3. Influence in detail of the degree of chaos of the input signal on the state of the driven Duffing oscillator

As Logistic map is only related with the bifurcation parameter k, it is convenient to make use of Logistic map to investigate the relationship between the degree of chaos of input signals and the state of Duffing oscillator. Figure 7 shows the bifurcation pro-

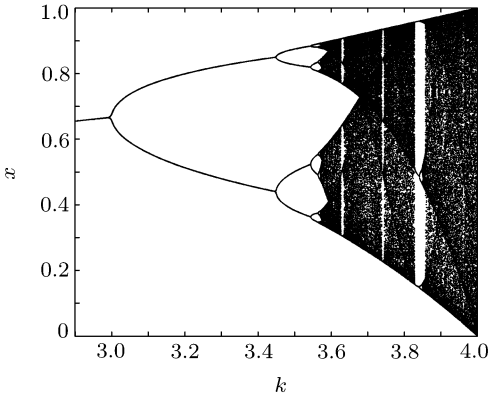


Fig.7. Bifurcation diagram of Logistic map plotted by x versus k.

cess of Logistic map. When k increases from 1 to 4, Logistic map transits from periodic state to chaotic state. The number of bifurcation times corresponding to a certain value of k indicates the degree of chaos of Logistic map. When $k = 3.569$, Logistic map begins to go into chaotic state; when $k = 4$, Logistic map is in completely chaotic state. The output signals of Logistic map with k taken as 3.5, 3.6, 3.7, 3.8, 3.9 and 4.0 are put into Duffing oscillator respectively, and the corresponding phase plane diagrams of Duffing oscillator are shown in Fig.8, which shows that the degree of chaos of the phase plane of Duffing oscillator increases as k increases.

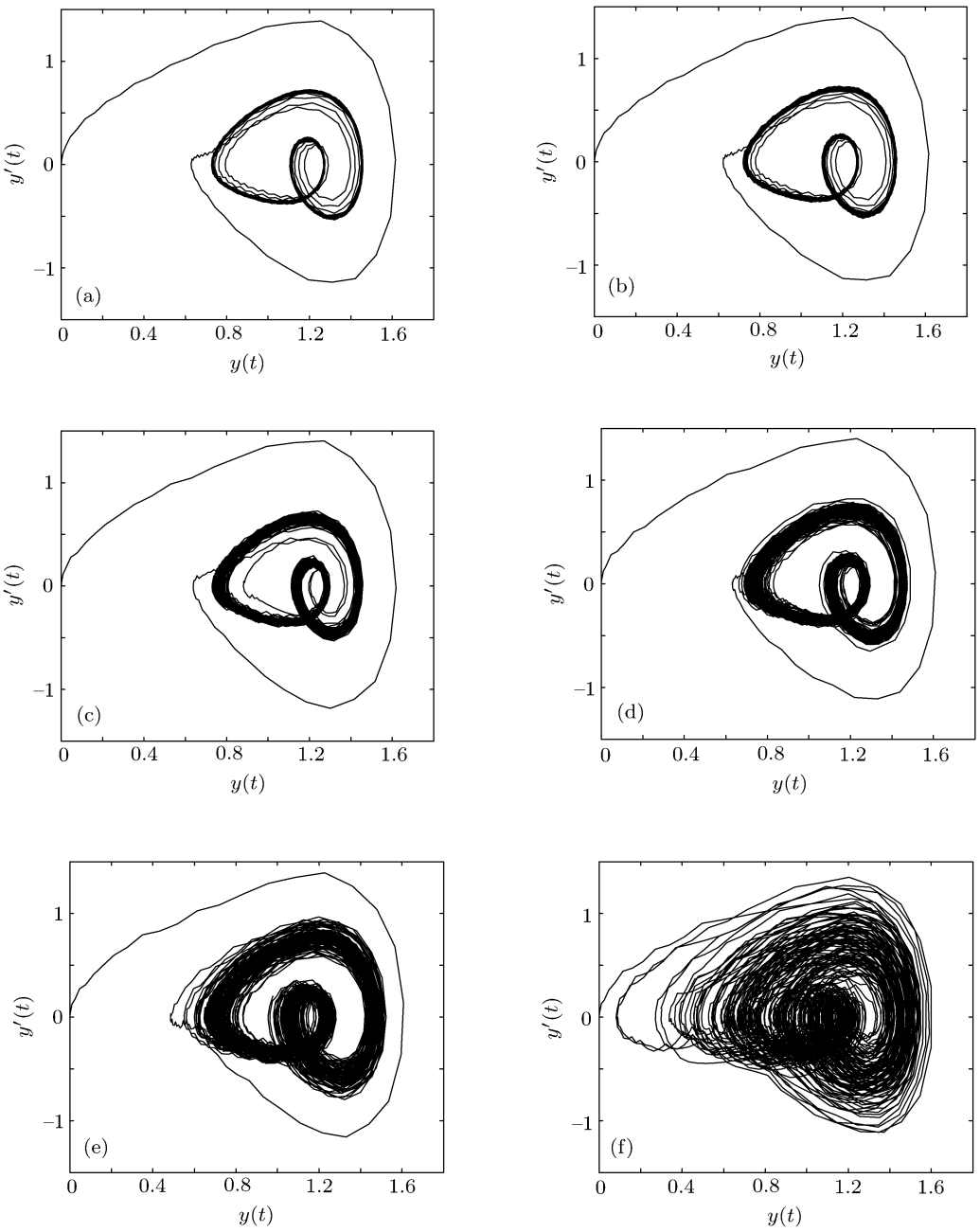


Fig.8. Phase plane diagrams of the driven Duffing oscillator with the output time series of Logistic map as input signal when the parameter k of Logistic map are taken as 3.5 (a), 3.6 (b), 3.7 (c), 3.8 (d), 3.9 (e) and 4.0 (f), respectively.

The LLE values of the output signals of Logistic map with different k values and the corresponding $y(t)$ are computed. As shown in Table 3, when $k = 3.5$, the LLE value of the output signal of Logistic map is negative, that is, Logistic map is in periodic state at this point, and the corresponding output signal is a periodic time series. When $k > 3.569$, Logistic map begins to go into chaotic state, and the degree of chaos of Logistic map becomes higher and higher as k increases up to $k = 4.0$, at which the Logistic map is in completely chaotic state.

Table 3. LLE for the output time series of Logistic map with different bifurcation parameter k and the corresponding output signals of the driven Duffing oscillator.

k	LLE	
	output signal of Logistic map	$y(t)$
3.5	–0.8725	–0.0052
3.6	0.1853	–0.0015
3.7	0.3459	0.0109
3.8	0.4482	0.0158
3.9	0.5012	0.0242
4.0	0.6932	0.0372

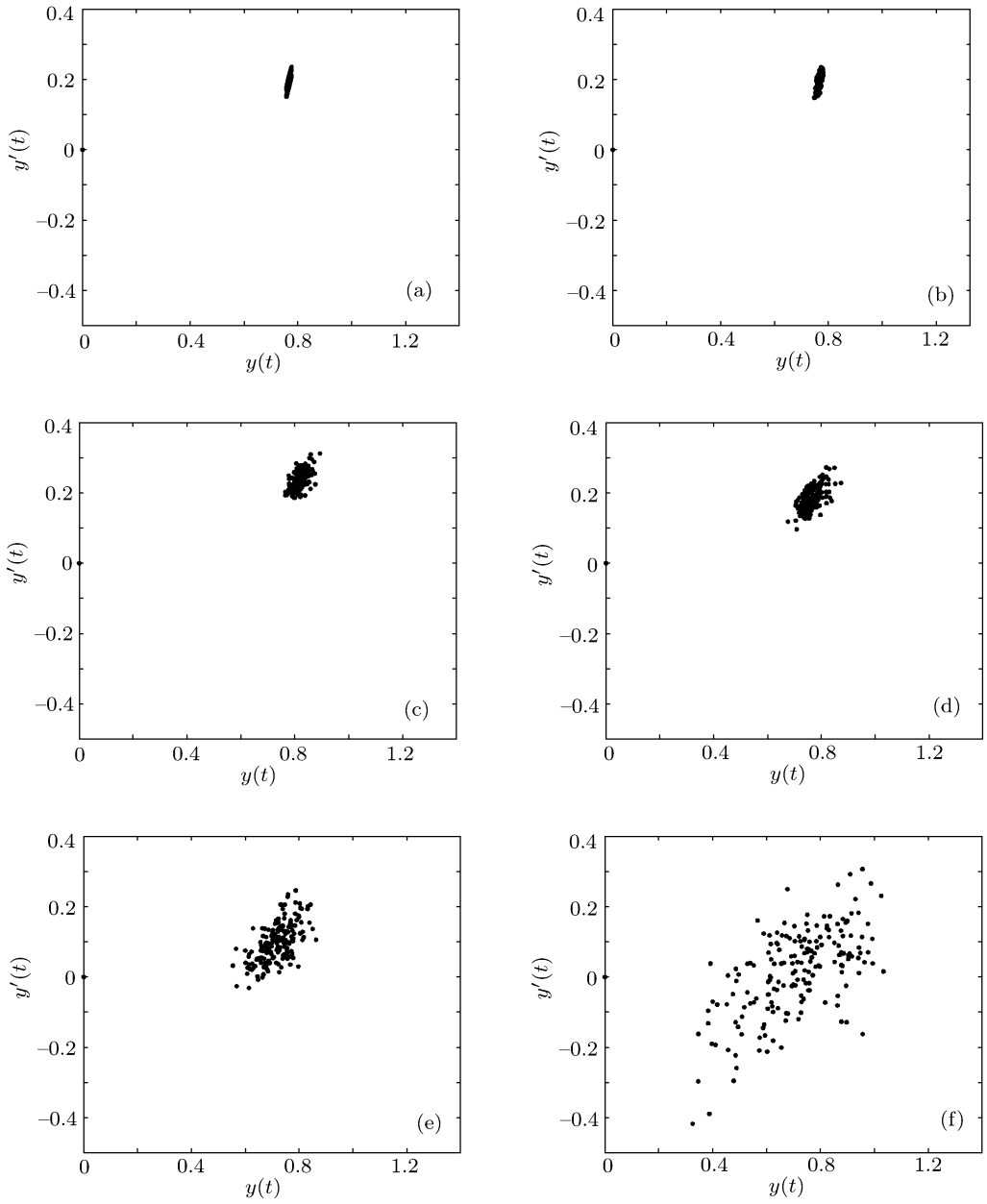


Fig.9. Poincaré section diagrams of the driven Duffing oscillator with the output time series of Logistic map as input signal when the parameter k of Logistic map are taken as 3.5 (a), 3.6 (b), 3.7 (c), 3.8 (d), 3.9 (e) and 4.0 (f), respectively.

We compare the phase plane diagrams shown in Fig.8 with the corresponding LLE values shown in Table 3. When $k = 3.5$, after the output signal of Logistic map in periodic state is put into Duffing oscillator, Duffing oscillator transits from transient chaotic state into stable periodic state because of the sensitivity of Duffing oscillator to (quasi-) periodic signals, the corresponding negative LLE value of $y(t)$ also proves the periodic state of the driven Duffing oscillator here. When $k = 3.6$, Logistic map shows low degree of chaos, but is still close to periodicity, since the bifurcation time with $k = 3.6$ shown in Fig.7 is limited. Therefore, the degree of chaos of the output signal of Logistic map at this point is not strong enough to drive Duffing oscillator to the chaotic state, the output signal of Logistic map only disturbs the phase plane of Duffing oscillator lightly, and the LLE result of $y(t)$ corresponding to $k = 3.6$ shows that Duffing oscillator is still in periodic state, which is close to chaotic state. After k becomes larger than 3.6, the degree of chaos of the output signal of Logistic map is high enough to drive Duffing oscillator to chaotic state, the LLE value of $y(t)$ becomes positive, which indicates that the Duffing oscillator is in chaotic state, and the LLE value of $y(t)$ increases as the LLE value of the output signal of Logistic map increases, that is, the degree of chaos of Duffing oscillator increases as the degree of chaos of input signal increases. The Poincaré section diagrams of Duffing oscillator with the output signals of Logistic map as input are also plotted. As shown in Fig.9, the Poincaré section diagrams clearly show the process that the state of Duffing oscillator transits from periodic to chaotic as the degree of chaos of the input signal increases.

5. A potential application of the new feature of the driven Duffing oscillator

Epilepsy is characterized by unexpected recurrent and transient disorder of mental function and movements of the body. It results from the excessive discharging of groups of brain cells.[26,27] Detection of abnormal EEG activity plays a significant role in the diagnosis of epilepsy. In recent years, many indexing methods, such as LLE,[21,22] approximate entropy,[28] correlation dimension,[22,29] time-varying dimension,[30] and permutation entropy,[31] have been developed to detect or predict epileptic seizure and achieved good results. The feature in common of these methods is that they all compare the characteristic quantities extracted from normal and epileptic EEG signals to detect or predict epileptic seizure. For example, the LLE values of EEG signals during epileptic seizure become smaller than those of normal EEG signals. Similar as observed from the results of the numerical experiments shown in the previous section, Duffing oscillator shows obviously different phase plane responses to normal and epileptic EEG signals. It is convenient and obvious to distinguish between normal and epileptic EEG signals based on the phase plane diagrams of Duffing oscillator. Therefore, the method based on the new feature of Duffing oscillator for detecting epileptic seizure is proposed initially. Figure 10 shows some supplementary phase plane diagrams of Duffing oscillator corresponding to the EEG signals, which are recorded together with the EEG signals used in the previous section but from different scalp electrodes. The phase plane diagrams shown in Fig.10 are similar with those shown in Fig.4, which illustrates that the different phase-state response of Duffing oscillator to normal and epileptic EEG signals is not occasional. The potential application of the new feature of the driven Duffing oscillator recommended in this paper for detecting epileptic seizure, which is different from the indexing methods of comparing the characteristic quantities extracted from normal and epileptic EEG signals, makes use of the difference of degree of chaos of phase plane of Duffing oscillator aroused by the difference of chaoticity between normal and epileptic EEG signals.

Because of the immunity of Duffing oscillator to random noise, it is not needed to pre-denoise the raw EEG signals, which makes the detection process simpler. As the structure of Duffing oscillator is not complex compared with the indexing methods, the running time of the method based on the new feature of Duffing oscillator to detect epileptic seizure is so short as can even be ignored, hence it is easy for this method to meet the real-time requirements. The low computation load, visualization of the results and no need of pre-denoising are the advantages of the method based on the new feature of Duffing oscillator for detecting epileptic seizure.

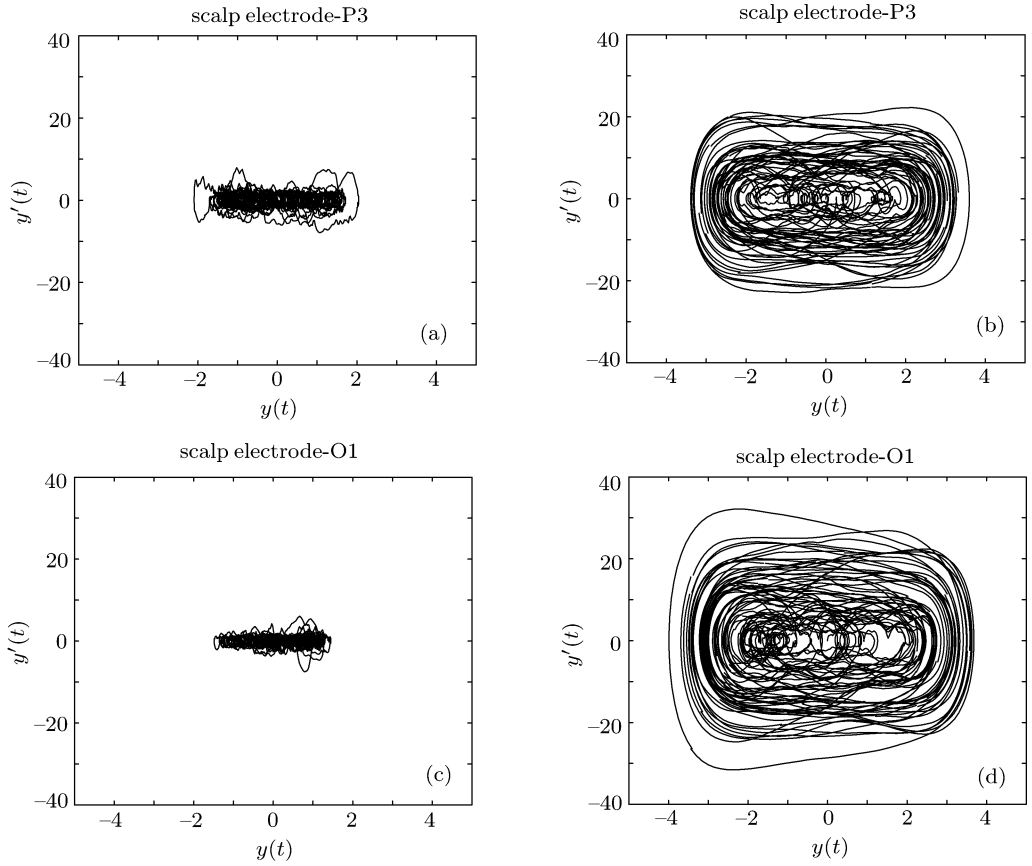


Fig.10. Supplementary phase plane diagrams of the driven Duffing oscillator, (a) and (c) correspond to normal EEG, (b) and (d) correspond to epileptic EEG. EEG signals for (a) and (b) were taken from the scalp electrode with the same index, P3. EEG signals for (c) and (d) were taken from the scalp electrode with the same index, O1.

6. Conclusion

We have disclosed a new feature of the driven Duffing oscillator, i.e., its regular nonlinear response to time series with different degrees of chaos. The results of numerical experiments on two artificial and one real-world time series showed clearly that the higher the degree of chaos of the input signal, the more chaotic the state of the driven Duffing oscillator is. We proposed a potential application of the new feature of the driven Duffing oscillator based on the results of the numerical experiments on EEG signals as well. The method based on the new feature of the driven Duffing oscillator for the detection of epileptic seizure still needs further research to be suitable for different types of seizure. Despite this, the method indicates the potential application of the new feature of the driven Duffing oscillator.

Acknowledgements

The authors thank Nicanor A Matias and Lijie Yu for many constructive suggestions.

References

[1] Lorenz E N 1963 *J. Atmos. Sci.* **20** 130
[2] Haykin S and Li X B 1995 *Proc. IEEE* **83** 95
[3] Wang Y C, Zhao Q C and Wang A B 2008 *Chin. Phys.* B **17** 2373
[4] Zheng S Y, Guo H X, Li Y A, Wang B H and Zhang P Y 2007 *Chin. Sci. Bull.* **52** 1906
[5] Yan Z, Guang Z H and De Z C 2008 *Chin. Phys.* B **17** 529
[6] Guo L W, Wei Z L and Ming L Q 2007 *Chin. Phys.* **16** 3256
[7] Qiang W F and Xin L C 2006 *Chin. Phys.* **15** 963
[8] Liu Z 1994 *Perturbation Criteria For Chaos* (Shanghai: Shanghai Scientific and Technology Education)

[9] Brown R, Chua L O and Popp B 1992 *Int. J. Bifurc. Chaos* **2** 193
[10] Birx D L and Pipenberg S J 1992 *IEEE Int. Joint Conf. Neural Netw.* **2** 881
[11] Wang G Y, Chen D, Lin J and Chen X 1999 *IEEE Trans. Ind. Electron.* **46** 440
[12] Wang G Y, Zheng W and He S L 2002 *Signal Processing* **82** 103
[13] Wang G Y and He S L 2003 *IEEE Trans. Circuits-I* **50** 945
[14] Li Y and Yang B J 2003 *Chin. Sci. Bull.* **48** 508
[15] Li Y, Yang B J, Zhao X P, Zhang M and Lin H B 2005 *Chin. J. Geophys.* **6** 1428
[16] Li Y, Yang B J, Yuan Y, Zhao X P and Lin H B 2006 *Chin. Sci. Bull.* **51** 3010
[17] Pradhan N and Sadasivan P K 1996 *Phys. Rev.* E **53** 2684
[18] Govindan R B, Narayanan K and Gopinathan M S 1998 *Chaos* **8** 495
[19] Norbert M, Niels W, Udo M, Alexander S and Jürgen K 2002 *Phys. Rev.* E **66** 026702
[20] Porcher R and Thomas G 2001 *Phys. Rev.* E **64** 010902
[21] Iasemidis L D, Dengshan S, Chaovalitwongse W, Sackellares J C, Pardalos P M, Principe J C, Carney P R, Prasad A, Veeramani B and Tsakalis K 2003 *IEEE Trans. Biomed. Eng.* **50** 616
[22] Adeli H, Ghosh-Dastidar S and Dadmehr N 2007 *IEEE Trans. Biomed. Eng.* **54** 205
[23] Izrailev F M, Timmermann B and Timmermann W 1988 *Phys. Lett.* A **126** 405
[24] Dettmer R 1993 *IEE Rev.* **39** 199
[25] Wolf A, Swift J, Swinney H and Vastano J 1985 *Physica* D **16** 285
[26] Jeong J, Kim M S and Kim S Y 1999 *Phys. Rev.* E **60** 831
[27] Yuan Y, Li Y and Mandic D P 2008 *J. Physiol. Sci.* **58** 239
[28] Srinivasan V, Eswaran C and Sriraam N 2007 *IEEE Trans. Inf. Technol. Biomed.* **11** 288
[29] Silva C, Pimentel I R, Andrade A, Foreid J P and Ducla-Soares E 1999 *Brain Topogr.* **11** 201
[30] Scott V N and Stephen J E 2003 *IEEE Trans. Biomed. Eng.* **50** 594
[31] Li X L, Ouyang G X and Richards D A 2007 *Epilepsy Res.* **77** 70